The Use of Land Surface Temperature Observations for the Assessment of Land Surface Parameterizations

Isabel F. Trigo and Pedro Viterbo

Instituto de Meteorologia, IP, Lisboa, Portugal / IDL,
University of Lisbon, Lisbon, Portugal
isabel.trigo@meteo.pt

Abstract

Land Surface Temperature estimated from Meteosat Second Generation (MSG) is used to assess ECMWF skin temperature, a variable which can be interpreted as a radiative temperature of the model surface. It is shown that the ECMWF model tends to slightly overestimate skin temperature during night-time and underestimate daytime values. Such underestimation of daily amplitudes is particularly pronounced in arid and semi-arid regions. The introduction of monthly fields of the leaf area index leads to a consistent positive impact on the model skin temperature, mostly associated to an overall reduction in the evaporative fraction. Such changes are more evident for forecasts experiments without assimilation. On the other hand, the revision of model roughness lengths for momentum and heat is shown to have a pronounced positive impact on the bias of daytime skin temperatures, particularly in areas which are not affected by changes in the model vegetation.

1. Introduction

Remote sensing estimations of Land Surface Temperature (LST) generally correspond to the directional radiometric temperature of the surface measured within the sensor direction. LST is routinely estimated from a wide range of sensors. Most remote sensing LST products make use of measurements within the atmospheric window in the thermal infra-red provided by sensors onboard polar-orbiters or geostationary satellites. The former provide global coverage and higher spatial resolution than the latter. However, a good sampling of the diurnal cycle of surface temperatures over land can only be achieved with data from geostationary platforms. Currently, the EUMETSAT Satellite Application Facility on Land Surface Analysis (LSA SAF) provides 15-minute LST for clear sky conditions from the Spinning Enhanced Visible and Infrared Imager (SEVIRI) onboard Meteosat Second Generation (MSG).

Remotely sensed LST may be used to assess model surface parameterizations over land, given the number of factors (e.g., soil moisture, available radiation, vegetation cover and state, orography) that affect model skin temperature. This generally corresponds to the temperature of the interface between the soil and the atmosphere, being close to a radiometric temperature of the surface, and therefore to satellite LST, when the thermal capacity of this interface is negligible.

Over land, model skin temperature is strongly influenced by the total radiation reaching the surface and also by all variables and model parameters that control surface energy fluxes, most notably: soil moisture; vegetation fraction and state; near-surface wind; roughness lengths for heat and momentum. The assessment of model skin temperature may provide useful information on the impact of changes in any of those topics. Here we use SEVIRI LST estimations to assess ECMWF operational forecasts of skin temperature, as well as the impact of changes in the model prescribed vegetation and roughness lengths for heat and momentum on skin temperature biases.

2. Remote Sensing of Land Surface Temperature

Land Surface Temperature (LST) is estimated on an operational basis by the LSA SAF (Trigo et al., 2011; http://landsaf.meteo.pt), from the Spinning Enhanced Visible and Infrared Imager (SEVIRI) onboard Meteosat Second Generation (MSG). LST retrievals are performed for clear sky pixels within the MSG disk, at the original pixel resolution (3 km at sub-satellite point) and with a 15-minute temporal sampling, which allows for a detailed representation of the surface temperature diurnal cycle. LST is obtained by correcting top-of-atmosphere (TOA) radiances for surface emissivity, atmospheric attenuation along the path and reflection of downward radiation. The LST algorithm follows closely the generalized split window proposed by Wan and Dozier (1996) for AVHRR and MODIS, but adapted to SEVIRI data (Trigo et al. 2008a, Freitas et al., 2010). LST (Fig. 1, left panel) is estimated as a regression of clear-sky TOA brightness temperatures for the split-window channels 10.8μm and 12.0μm, and of land surface emissivity for each channel. The split-window parameters were finely adjusted for classes of atmospheric water vapour content and satellite viewing angle (Freitas et al., 2010). Channel and broadband emissivity is estimated as a weighted average of that of bare ground and vegetation elements within each pixel (Peres and DaCamara 2005; Trigo et al. 2008b), using the fraction of vegetation cover (FVC), another LSA SAF product retrieved operationally from SEVIRI/MSG.

The uncertainty of LST estimations depends on a number of factors (Freitas et al. 2010), including: (i) the retrieval conditions in terms of atmospheric water content and viewing geometry, since the total optical path will strongly influence the performance of the generalized split-window algorithm; (ii) input uncertainties, including sensor noise, errors in the estimation of surface emissivity and in atmospheric total water vapour obtained from ECMWF forecasts; and (iii) errors in the cloud mask used to identify clear sky pixels.

The validation of LST estimations is based on (i) comparisons with LST retrieved from other sensors (e.g., MODIS onboard Terra and Aqua); and (ii) comparison with in-situ measurements. The latter should be representative of the pixel scale, a requirement that is often difficult to meet. To overcome the scarcity of adequate in situ LST ground observations within the Meteosat disk, the LSA SAF set-up ground-truth stations in Évora, Southern Portugal (Kabsch et al., 2008; Trigo et al, 2008a), as well as in Namibia and Senegal.

Figure 1 (right panels) present examples of scatterplots of observations versus LST retrievals at Gobabeb (Namibia), for May and November 2008. This site is located within a fairly homogeneous area, characterized by gravel plains. The match between LSA SAF estimations and in situ observations is overall very good, with root mean square differences (RMS) between 1ºC and 2ºC. The discrepancies in sites characterized by more heterogeneous landscapes, such as Évora, present larger differences, but generally with RMS within 2.5ºC (Trigo et al, 2008a).

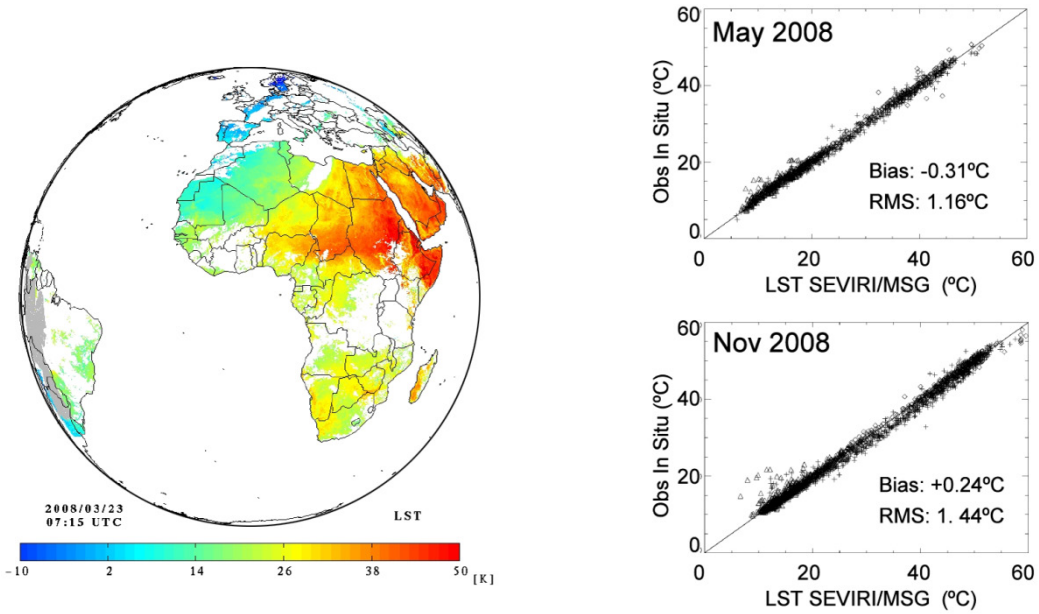

Figure 1: Left panel: LST field retrieved from SEVIRI/MSG on the 23rd of August 2008; 7:15 UTC time slot; white pixels do not have a retrieved value (ocean or cloudy pixels), while grey pixels were masked out due to the high uncertainty of the estimations (4K or higher). Right panels: Comparison between LST SEVIRI estimations (x-axis) and in situ observations (y-axis) taken at Gobabeb (Namibia,) during May 2008 (top) and November 2008 (bottom); bias and root mean square differences between SEVIRI estimations and ground measurements are also indicated.

3. Model Skin Temperature

The skin temperature corresponds to the temperature of the interface between the soil and the atmosphere. In ECMWF model, this interface is modelled by the Hydrology Tiled ECMWF Scheme for Surface Exchanges over Land (HTESSEL) (Balsamo et al., 2009). Within HTESSEL, each grid-box is split into fractions of a set of possible surface types, or tiles, namely: bare ground, low and high vegetation, intercepted water, shaded and exposed snow, over land; and open and frozen water, for sea and inland water surfaces (e.g. Viterbo and Beljaars 1995). The skin temperature (Tskin) of each tile is determined as the solution for the respective surface energy balance equation, while ECMWF skin temperature is then estimated as the weighted average of tile Tskin. Considering that the soil-atmosphere interface has no thermal inertia, then Tskin is essentially the radiometric temperature of the model surface, and therefore very close to infrared remote sensing retrievals.

Over land, model skin temperature is strongly influenced by the total radiation reaching the surface and also by all variables and model parameters that control surface energy fluxes, most notably: soil moisture; vegetation fraction and state; near-surface wind; roughness lengths for heat and momentum. The assessment of model skin temperature may provide useful information on the impact of changes in any of those topics.

3.1. ECMWF operational model – evolution

A first comparison between model and Meteosat-7 and Meteosat-5 observations was carried out for the period between February and October 2001 (Trigo and Viterbo, 2003). The study was focused on modelled TOA brightness temperatures for the 11μm channel, which under clear sky conditions is essentially driven by surface temperature. Results put into evidence deficiencies in the cloud screening of the satellite data, particular in tropical regions, a problem that has been largely improved in SEVIRI/MSG radiances essentially due to the higher spectral and spatial resolutions. The work by Trigo and Viterbo (2003) revealed also a systematic underestimation of the diurnal cycle of model brightness temperature in clear-sky conditions with a cooling error during daytime of up to 7-8 K, and a much smaller and less widespread warming error at night.

Figure 2 presents the averaged difference between LSA SAF LST and ECMWF skin temperature forecasts for the period 1-15 January 2009, per observation times. The statistics are estimated once the LSA SAF LST data are aggregated to the model reduced gaussian grid by averaging pixels within each model grid-box. Since LST estimations are obtained for clear sky pixels only, all comparisons between model and remote sensing estimations analysed here exclude all model simulations with total cloud cover higher than 10%.

The conclusion drawn above for 2001 TOA brightness temperatures largely applies to 2009 model skin temperatures: the underestimation of the diurnal cycle is still present, particularly over arid and semi-arid regions, associated to a slight under-cooling of the model during night-time and an underestimation of daytime temperatures.

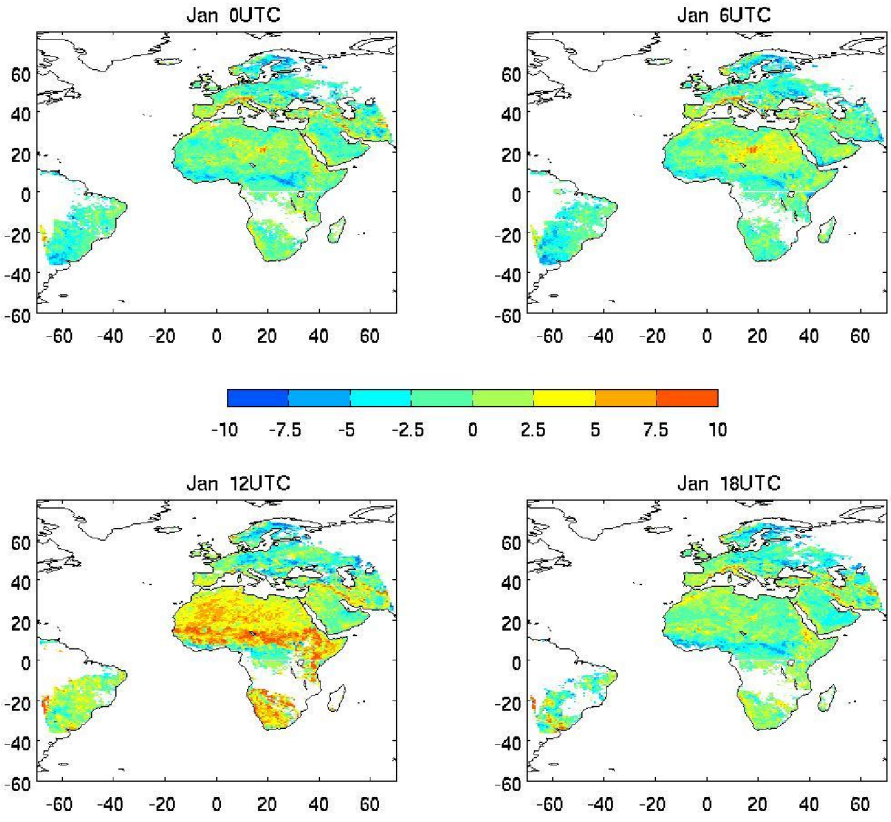

Figure 2: Difference between LSA SAF LST and model skin temperature (ºC) averaged for the period 1-15 January 2009 obtained using operational forecasts (12 to 30h time steps) for 0 UTC, 6 UTC, 12 UTC and 18 UTC, respectively, as indicated at the top of each panel.

It is worth mentioning that the overall results depicted in Fig. 2 are corroborated by comparisons with in situ observations. These are shown in Fig. 3 for Gobabeb site (Namibia), considering 3-hourly ECMWF skin temperature forecast and SEVIRI LST values; the latter were interpolated in space to ECMWF grid. Although overall ECMWF biases range from about -1 (October 2008) to -3 ºC (April 2009), it is clear that discrepancies are higher for daytime, with the model significantly underestimating the warmest observed temperature. A small overestimation of model night-time/early morning temperatures may also be detected in October and January panels.

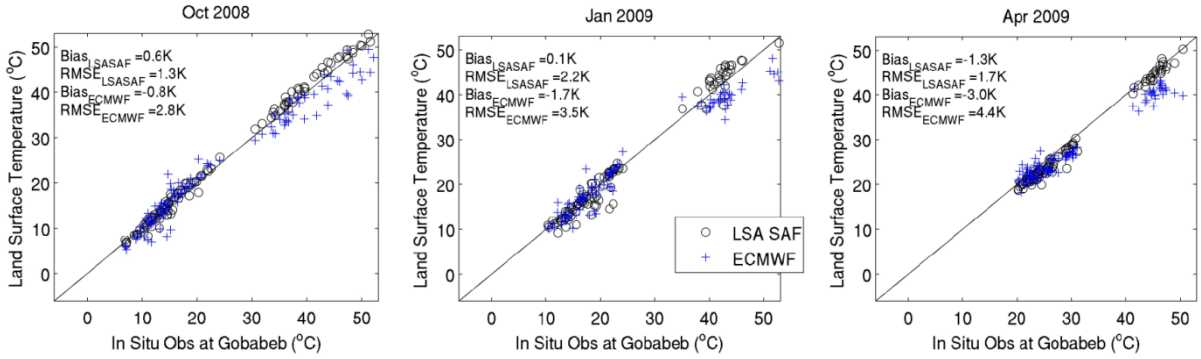

Figure 3: Scatterplots of ECMWF skin temperature (blue crosses) and LSA SAF LST estimations (black circles) versus in situ observations at Gobabeb (Namibia). Only ECMWF and LSA SAF data collocated in space and time are considered, i.e. 3-hourly data over a 25 km ECMWF model resolution.

3.2. Impact of Model Vegetation

Leaf Area Index (LAI) is a dimensionless variable (m2/m2) defined as one half of the total leaf area per unit ground area, therefore accounting for the surface of leaves contained in a vertical column. In land surface models, LAI is often used as indicator of the vegetation state, which in turn is an essential factor controlling the partition between sensible and latent energy fluxes over land (e.g., Seneviratne et al., 2010).

Currently, ECMWF model is still using an LAI map constant in time (Fig. 4, top panel), which is essentially a function of the grid box land cover type. Overall, LAI presents a strong seasonal cycle reflecting the yearly vegetation development and decay. In this section we analyse the impact on skin temperature of introducing a monthly-dependent LAI into ECMWF model. For that purpose, we consider the output of the experiments described in Boussetta et al. (2012), comprising both forecast and assimilation experiments, where ECMWF model constant LAI is replaced by satellite-based global monthly climatologies (Table 1). These are based on data collected by two different sensors: the Moderate Resolution Imaging Spectro-radiometer (MODIS); and the Advanced Very High Resolution Radiometer (AVHRR) used to build the ECOCCLIMAP database.

An additional set of experiments (see f8mu and f8o5 in Table 1) was carried out, where the original LAI was modified to MODIS monthly climatology and the values of minimum stomatal resistance were revised for crops (from 180 to 100 sm^{-1}), short grass (from 110 to 100 sm^{-1}) and needle-leaf trees (from 500 to 250 sm^{-1}) in an attempt to compensate for biases in two-metre humidity associated to the LAI changes (Boussetta et al., 2012).

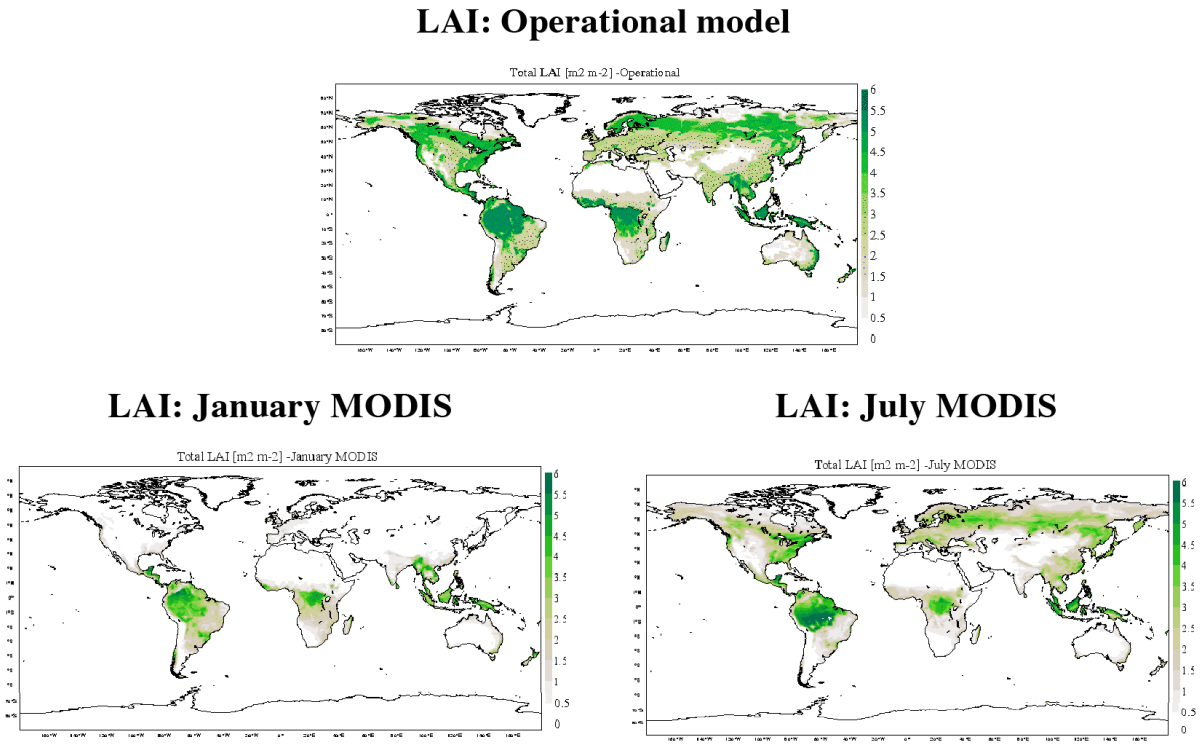

Figure 4: Total LAI (m^2/m^2) as defined in the operational model (top panel); lower panels show the MODIS LAI climatology for January and July, respectively (G. Balsamo, personal communication).

Table 1: Experiments considered for the LAI impact assessment (Boussetta et al., 2012).

Type	Experiment id	Period	Resolution	Description
Forecast	F7wx	20080101-20090101	T399	Control (constant LAI)
	F7vr			LAI from ECOCLIMAP
	F87n			LAI from MODIS
	F8mu			LAI from MODIS + minimum stomatal resistance adjustment
Assimilation + Forecast	F85e	20080214-20080901	T255	Control (constant LAI)
	F85f			LAI from ECOCLIMAP
	F8o5			LAI from MODIS + minimum stomatal resistance adjustment

The bias of the control experiment obtained for 0 UTC and 12 UTC for May is shown in Fig. 5. Again, this suggests a fairly good agreement of night-time temperatures and an underestimation of daytime temperature by the model. A similar picture is obtained for other months, although the magnitude of the daytime discrepancies tends to be larger during summer in mid-latitudes / dry season in the sub-tropics. It should be pointed out that the uncertainty of LST estimations increases significantly for large viewing angles. Therefore, the large biases in areas near the edge of Meteosat disk (e.g., Arabian Peninsula, Scandinavia) must be dealt carefully and will not be considered here.

The impact on skin temperature of MODIS LAI (experiment f87n) and of MODIS LAI along with the revision to minimum stomatal resistance is shown in Fig. 6 for daytime temperatures (March-to-May 2008). The impact is measured in terms of the difference in the mean absolute error of the control versus experiment (i.e., a positive impact corresponds to a lower absolute error in the experiment). SEVIRI LST is being used here as reference for skin temperature. Figure 6 puts into evidence wide areas with positive impact, mostly over the Sahel, the Southern part of Africa and most of Europe. As expected, areas without vegetation, such as the Sahara, remain unaffected. The impact for the experiment with the adjustment of the stomatal resistance over Europe is attenuated when compared with that of MODIS LAI. Although not shown, the impact on daytime skin temperature is negative over Europe during summer, when minimum stomatal resistance is reduced (particularly in areas with significant coverage of needle-leaf trees). The impact on night-time skin temperature of the experiments under analysis is very small (not shown), less than 0.5 - 0.25ºC for most regions.

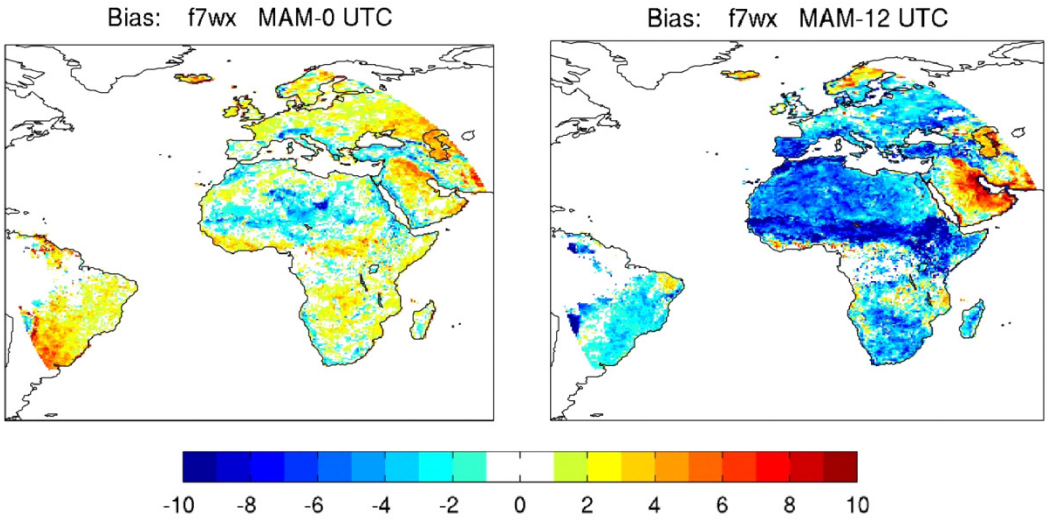

Figure 5. Skin temperature bias with respect to SEVIRI LST (ECMWF minus SEVIRI LST; ºC) obtained for the control forecast experiment for 0UTC (left) and 12 UTC (right panel) for March-April-May 2008.

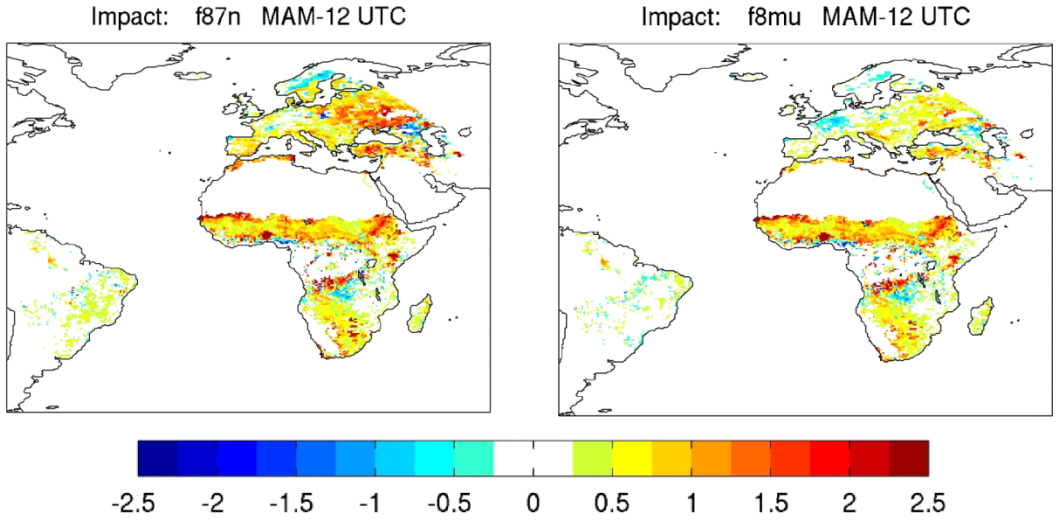

Figure 6. Impact on model skin temperature (ºC) obtained for experiments: with MODIS LAI (left); with MODIS LAI and minimum stomatal adjustment (right). Both panels refer to 12 UTC, March-April-May 2008.

The introduction of a more realistic representation of vegetation in ECMWF model led to an overall decrease in LAI values with a pronounced seasonal cycle (Fig. 4). As shown in Fig. 7, this seems to be associated to a general decrease in the evaporative fraction, mostly driven by a reduction in evapotranspiration. Sensitivity values shown in Fig. 7 are estimated as the evaporative fraction of experiments minus that of the control.

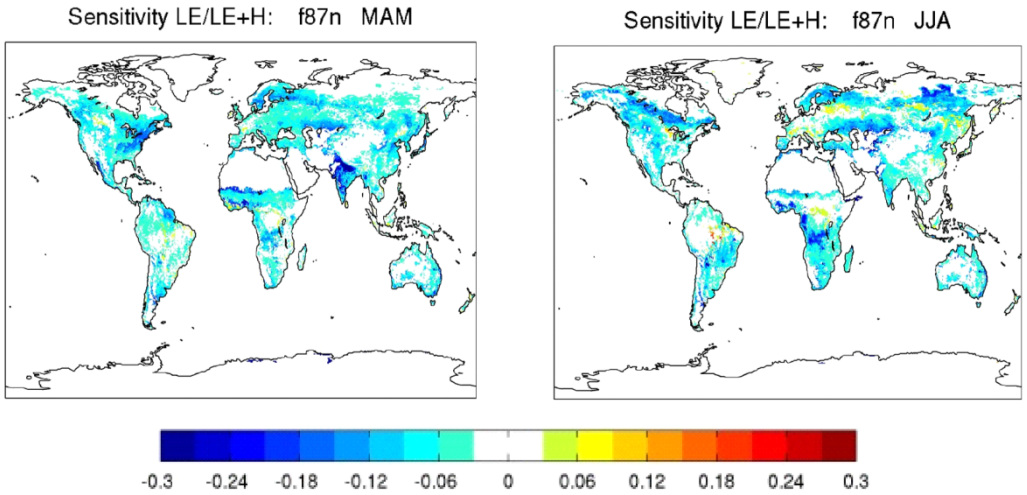

Figure 7. Sensitivity of daily evaporative fraction for experiment with MODIS LAI for March-April-May (left); and June-July-August (right).

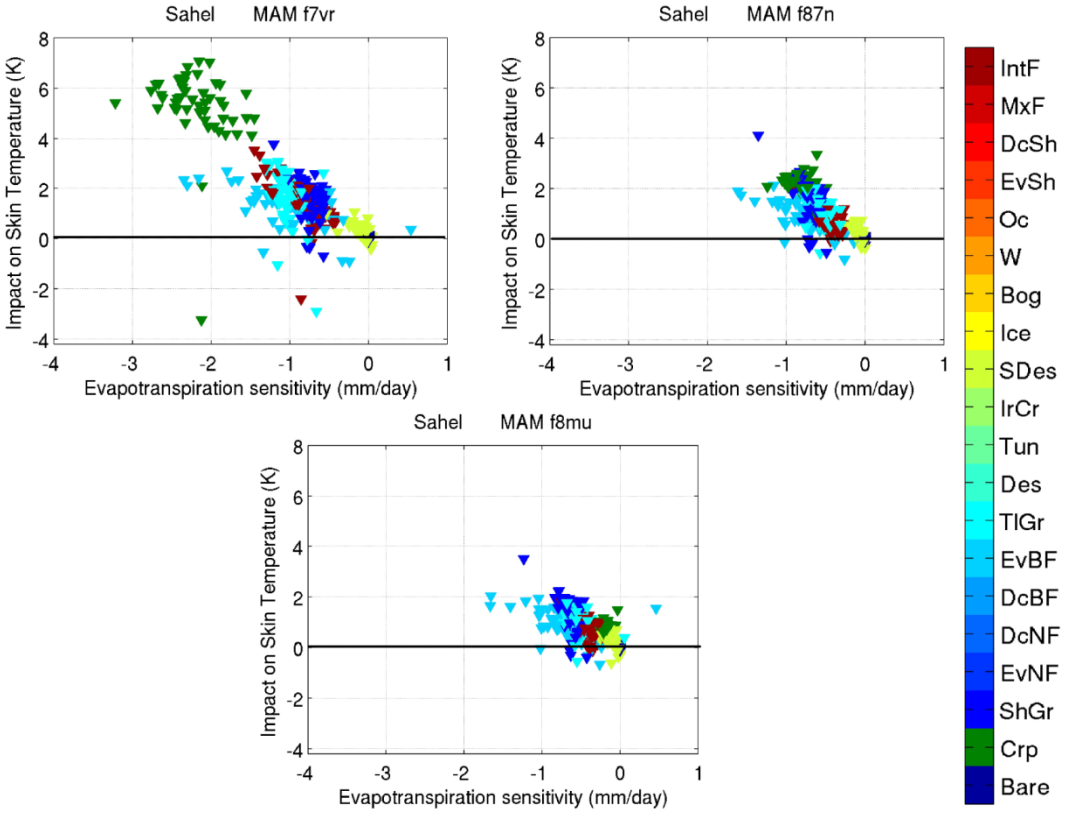

Figure 8: Scatter plots of the impact on 12 UTC skin temperature (ºC) versus sensitivity of daily evapotranspiration (mm/day) for the Sahel and for the following experiments: ECOCLIMAP LAI (top left); MODIS LAI (top right) and MODIS along with the revised minimum stomatal resistance (bottom). All plots correspond to the period March-April-May 2008 and the dots are coloured according to the model dominant land cover type.

The positive impact on model daytime skin temperature is clearly associated to the decrease in evapotranspiration introduced by the new LAI values, as shown in Fig. 8. Furthermore, Fig. 8 puts into evidence the variability among different land cover types and between ECOCLIMAP and MODIS LAI.

In all the experiments discussed so far, the initial soil moisture is the same in the control and in the model run with the modified vegetation. In data assimilation experiments, soil moisture responds to evaporative changes during the assimilation process, i.e., less evaporation is most places will lead to a wetter soil for the next background. As a consequence, the impact of changes in the model LAI are significantly attenuated during the subsequent forecast (Fig. 9), since a wetter soil partly compensates for the model induced changes in the evaporative fraction.

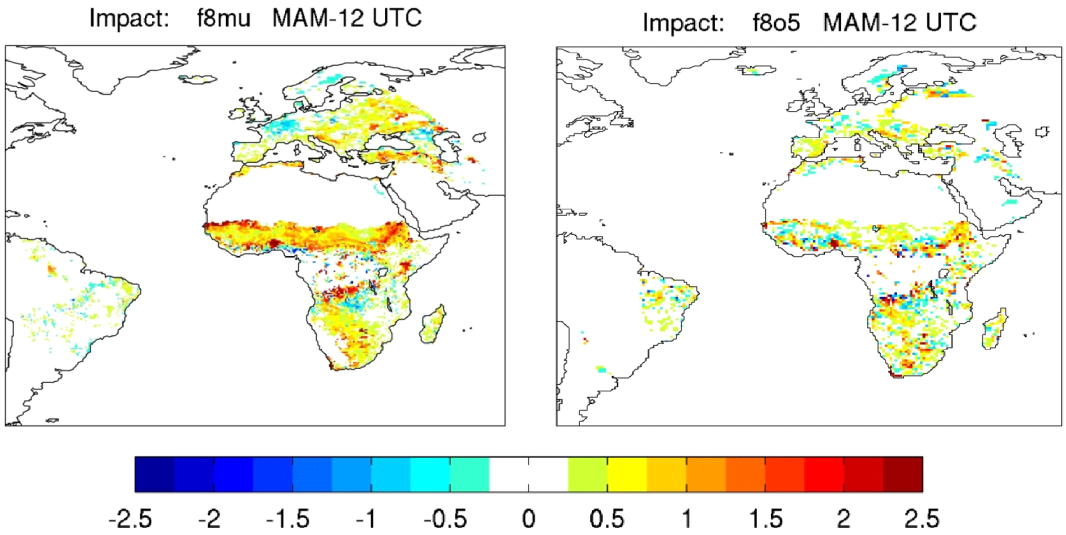

Figure 9: Impact on model skin temperature (ºC) obtained for experiments with MODIS LAI and minimum stomatal adjustment: forecast experiment (left); and assimilation experiment (right). Both panels refer to 12 UTC, March-April-May 2008.

3.3. Impact of Model Surface Roughness

In this section we analyse the impact of changes in the surface roughness for momentum (Z_{oM}) and heat (Z_{oH}) on the model skin temperature. ECMWF operational forecasts generally overestimate 10m wind. A set of experiments was then carried out using a new table of surface roughness length for momentum, Z_{oM}, adjusted in order to compensate 10m wind biases for different tiles (I. Sandu, personal communication). The estimation of the revised roughness lengths assumed neutral wind profiles for all tiles (Table 2). Roughness lengths for heat in ECMWF operational model are prescribed as 10% of Z_{oM} for all tiles, except in forest areas, where $Z_{oH} = Z_{oM}$. Since revised values of Z_{oM} are decreased for most surface types, the ration between Z_{oM} and Z_{oH} is increased to 100 for all tiles, except for forests and ice caps, where both roughness lengths are kept equal (Table 2). The increase in the Z_{oM} / Z_{oH} ratio results in an enhanced resistance to heat transfer likely to be associated to the high spatial heterogeneity of land surfaces, which in turn brings model and observed TOA brightness temperatures closer (Sandu, personal communication).

The set of experiments analysed here are described in Table 3. These correspond to T511 forecasts initialized from their own analysis. The control experiment uses the original Z_{oM} and Z_{oH} values used at ECMWF, while in the remaining experiments these are replaced by the revised values (Table 2).

Table 2: Roughness lengths for momentum and for heat (I. Sandu, personal communication).

Surface Type	Original		New Values	
	Z_{oM} (m)	Z_{oH} (m)	Z_{oM} (m)	Z_{oH} (m)
Bare soil	0.013	0.0013	0.013	**0.00013**
Crops, mixed farming	0.15	0.015	**0.5**	**0.005**
Short grass	0.02	0.002	**0.2**	0.002
Evergreen needle-leaf trees	2	2	2	2
Deciduous needle-leaf trees	2	2	2	2
Deciduous broad-leaf trees	2	2	2	2
Evergreen broad-leaf trees	2	2	2	2
Tall grass	0.1	0.01	**0.47**	**0.0047**
Desert	0.013	0.0013	0.013	0.0013
Tundra	0.05	0.005	**0.034**	**0.00034**
Irrigated crops	0.15	0.015	**0.5**	**0.005**
Semidesert	0.05	0.005	**0.17**	**0.0017**
Ice caps	0.0013	0.00013	0.0013	0.00013
Bogs and marshes	0.05	0.005	**0.83**	**0.0083**
Inland water	0.0001	0.00001	0.0001	0.00001
Ocean	0.0001	0.00001	0.0001	0.00001
Evergreen shrubs	0.1	0.01	**0.37**	**0.0037**
Deciduous shrubs	0.1	0.01	**0.25**	**0.0025**
Mixed forest	2	2	2	2
Interrupted forest	0.5	0.5	**1.1**	**1.1**

Table 3: Experiments considered for the impact assessment of roughness lengths (I. Sandu, personal communication).

Type	Experiment id	Period	Resolution	Description
Assimilation + Forecast	fgth	20100201-20100228	T511	Control (original Z_{oM} and Z_{oH})
	fhqm			Revised Z_{oM} and Z_{oH}
	fhbk	20100802-20100831		Control (original Z_{oM} and Z_{oH})
	fhqk			Revised Z_{oM} and Z_{oH}

The impact of the revised roughness length table on the model skin temperature is shown in Fig. 10. This is negligible for night-time and positive for daytime conditions, particularly over arid regions. There the new Z_{oM} and Z_{oH} values lead to a significant reduction of the systematic underestimation of model daily amplitudes of skin temperature when compared to the remote sensed estimations. The map for 12 UTC in February (top right panel in Fig. 10) presents a very sharp north-south gradient over the Sahel, which seems to be clearly associated to the transition between land-cover classes (desert – semidesert – short-grass). The corresponding panel for August presents very pronounced positive impact values over northern Africa and to a lesser extent over Europe and Southern Africa. However, the impact is negative over the Western Sahara and the Arabian Peninsula. The statistics over the former area correspond to a very limited number of days (less than 5 in most cases), where both model and satellite observations are flagged as clear sky (in the case of ECMWF model this corresponds to grid boxes with total cloud cover of 10% or less). In the case of the Arabian region, we have both a relatively low number of clear sky conditions available and high uncertainty of LST estimation, due to the high SEVIRI viewing angles.

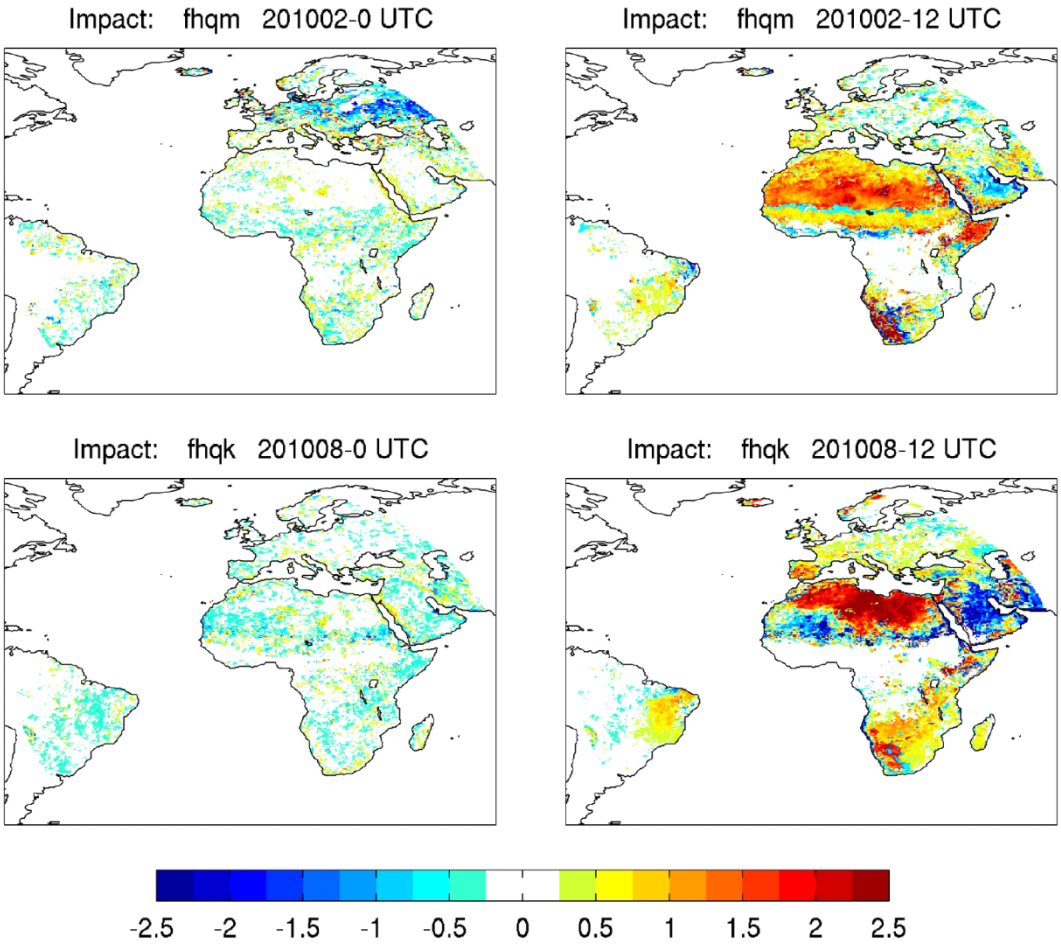

Figure 10: Impact of the revised roughness length table on skin temperature at 0 UTC and 12 UTC (left and right panels, respectively); for February 2010 and August 2010 (top and bottom panels, respectively).

The sensitivity of 10m wind speed at 12 UTC is shown in Fig. 11; again only clear sky situations are considered. As expected, wind decreases over most regions, as a consequence of the increased roughness length Z_{oM}. The reduction in near surface wind contributes to the increase in the aerodynamic resistance, and to lower heat fluxes. The Sahara and Arabian Peninsula, dominated by "desert" or "bare soil" tiles, with unchanged roughness lengths for momentum, do not present significant variation in wind speed between control and experiments. In those regions the positive impact on skin temperature is only associated to the reduction in roughness length for heat (Table 2) and associated increase in the resistance to heat transfer.

The combination of an overall decrease in near surface wind speed and Z_{oH} results in a generalised reduction in the model sensible heat flux (Fig. 12). Within the area covered by Meteosat disk, this reduction is enhanced over the regions where the impact on skin temperature is the largest. The sensitivity of latent heat flux to the revised table of roughness temperatures (not shown) is very small compared to that of sensible heat flux.

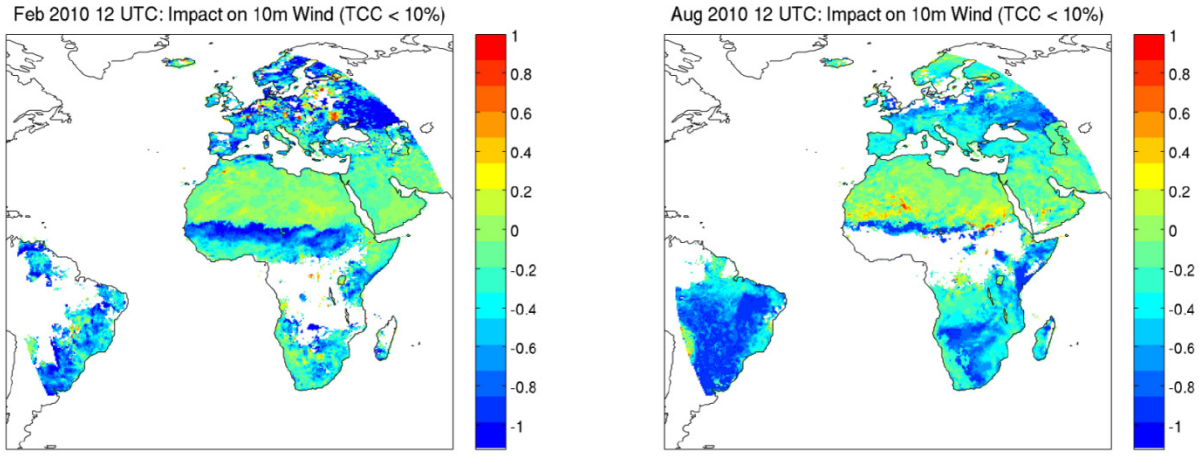

Figure 11. Sensitivity of 10 m wind speed at 12 UTC to the revised version of roughness lengths for February (left); and August (right).

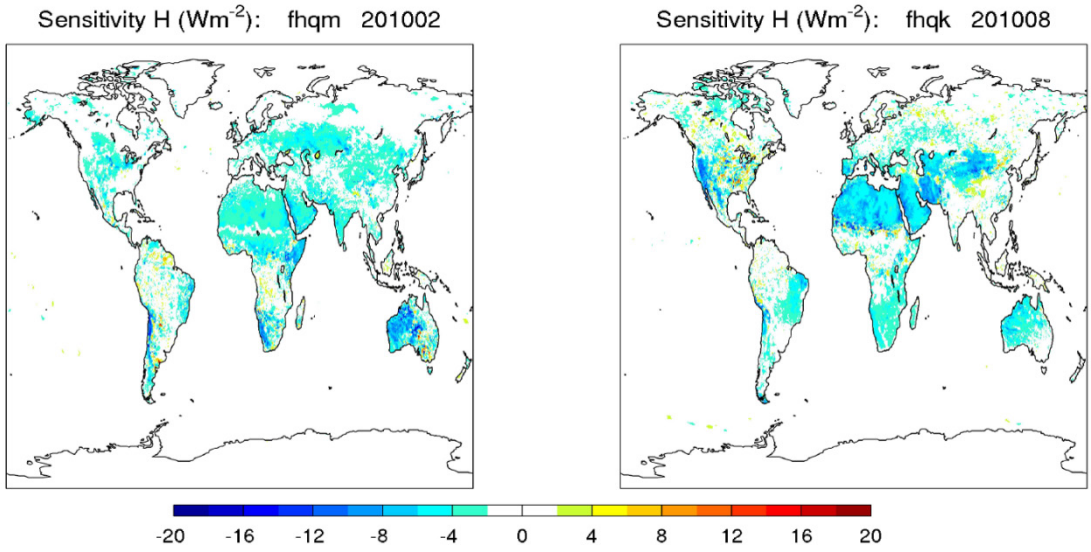

Figure 12. As in Fig. 11, but for daily sensible heat flux.

4. Concluding Remarks

Remotely sensed estimations based on SEVIRI/MSG at the original satellite spatial and temporal resolutions are estimated using a split-windows algorithm, trained to SEVIRI response functions. These data are produced, archived and disseminated by the LSA SAF produces, along with an estimation of the retrieval uncertainty on a pixel-by-pixel basis. Product validation is based on comparison against independent data sources, including both in situ measurements and similar parameters obtained from other sensors. The use of ground data is dependent on its representativeness of the pixel scale, an important limiting factor giving the high heterogeneity of land surfaces. Comparison of retrieved LST with observations at Evora (site in Southern Portugal) and at Gobabeb (Namibia) reveal discrepancies below 2ºC, generally within the estimated product uncertainty.

ECMWF model skin temperature is close to a radiative temperature of the surface, since it is estimated as the solution to the energy balance at the soil-atmosphere interface without heat capacity. Skin temperature forecasts produced by ECMWF operational model are overall cooler than SEVIRI LST retrievals during daytime and slightly warmer during night-time, leading to an underestimation of the skin temperature diurnal cycle. This is pronounced particularly in arid and semi-arid regions: Northern Africa, Sahel, and Southern Europe during the summer.

A set of forecast and assimilation experiments is presented, where the constant leaf area index (LAI) currently used by ECMWF operational model is replaced by monthly climatologies based on MODIS and AVHRR (ECOCLIMAP) LAI estimations. It is shown that this change contributes to reduce the bias of daytime skin temperatures mentioned above, although leaving out desert and semi-desert areas where vegetation cover is negligible. The increase in the daily amplitude of model skin temperature is associated to a general decrease in evaporative fraction. However, this positive impact on skin temperature is attenuated in the case of assimilation experiments. In this case, the analysed soil moisture is higher due to the lower evapotranspiration.

The adjustment of roughness lengths for heat and momentum leads to an overall positive impact on daytime skin temperature, generally associated to a reduction of sensible heat flux as a result of lower values of Z_{oH}. The positive impact is particularly relevant in non-vegetated areas that remained unaffected by the changes in the vegetation representation. In this case the positive impact is evident in forecast experiments from its own analysis.

References

Balsamo, G., P. Viterbo, A. Beljaars, B. Van den Hurk, A. K. Betts, and K. Scipal, 2009: A revised hydrology for the ECMWF model: Verification from field site to terrestrial water storage and impact in the Integrated Forecast System. *J. Hydrometeorol.*, **10**, 623–643 doi:610.1175/2008JHM1068.1171.

Boussetta, S., G. Balsamo, A. Beljaars, T. Kral and L. Jarlan, 2012: Impact of a satellite-derived Leaf Area Index monthly climatology in a global Numerical Weather Prediction model. *Int. J. Remote Sensing*, accepted.

Freitas, S. C., Trigo, I. F., Bioucas-Dias, J. M., Goettsche, F.-M., 2010: Quantifying the Uncertainty of Land Surface Temperature Retrievals From SEVIRI/Meteosat, *IEEE Trans. Geosci. Remote Sens.* DOI: 10.1109/TGRS.2009.2027697.

Kabsch, E., Olesen, F. S. and Prata, 2008: Initial results of the land surface temperature (LST) validation with the Evora, Portugal ground-truth station measurements. *Int. J. Remote Sensing*, **29**, 5329-5345.

Peres, L. F. and C. C. DaCamara, 2005: Emissivity Maps to Retrieve Land-Surface Temperature from MSG/SEVIRI, *IEEE Trans. Geosci. Remote Sens*., **43**, pp. 1834-1844, 2005.

Seneviratne, S.I., T. Corti, E.L. Davin, M. Hirschi, E.B. Jaeger, I. Lehner, B. Orlowsky, and A.J. Teuling, 2010: Investigating soil moisture-climate interactions in a changing climate: A review. *Earth-Science Reviews*, **99**, 125-161, doi:10.1016/j.earscirev.2010.02.004.

Trigo, I. F., C. C. DaCamara, P. Viterbo, J.-L. Roujean, F. Olesen, C. Barroso, F. Camacho-de Coca, D. Carrer, S. C. Freitas, J. García-Haro, B. Geiger, F. Gellens-Meulenberghs, N. Ghilain, J. Meliá, L. Pessanha, N. Siljamo, and A. Arboleda, 2011: The Satellite Application Facility on Land Surface Analysis. *Int. J. Remote Sens*., **32**, 2725-2744, doi: 10.1080/01431161003743199.

Trigo, I. F., I. T. Monteiro, F. Olesen, and E. Kabsch, 2008a: An assessment of remotely sensed land surface temperature, *J. Geophys. Res*., **113**, D17108, doi:10.1029/2008JD010035.

Trigo, I. F., L. F. Peres, C. C. DaCamara, and S. C. Freitas, 2008b: Thermal Land Surface Emissivity retrieved from SEVIRI/Meteosat. *IEEE Trans. Geosci. Remote Sens*., *IEEE Trans. Geosci. Remote Sens*., Doi: 10.1109/TGRS.2007.905197.

Trigo I. F., and P. Viterbo, 2003: Clear sky window channel radiances: a comparison between observations and the ECMWF model. *J. App. Met.*, **42**, 1463-1479.

Viterbo, P., and A.C.M. Beljaars, 1995: An improved land surface parametrization scheme in the ECMWF model and its validation. *J. Climate*, **8**, 2716-2748.

Wan, Z. and J. Dozier, 1996: A generalized split-window algorithm for retrieving land surface temperature from space, *IEEE Trans. Geosci. Remote Sens*., **34**, 892–905.